Research Square

Preprints are preliminary reports that have not undergone peer review.
They should not be considered conclusive, used to inform clinical practice,
or referenced by the media as validated information.

Mechanistic insights into the regulation of multi-scale structure and digestibility of pullulanase-debranched pea starch by oleic acid complexation

Wenjie Fu
Linyi University
Dong Kong
Linyi University
Hong Liu
Binzhou Inspection and Testing Center
Ziyu zhuang
Linyi University
Shanli Peng
Linyi University
Jiaojiao Yu
Linyi University
Hui Ji
hji8002@126.com
Linyi University

Research Article

Keywords: Pea starch, Debranched pea starch-oleic acid complex, In vitro digestibility

Posted Date: November 13th, 2026

DOI: https://doi.org/10.21203/rs.3.rs-11075068/v1

License: This work is licensed under a Creative Commons Attribution 4.0 International License.
Read Full License

Additional Declarations: No competing interests reported.

Mechanistic insights into the regulation of multi-scale structure and digestibility of pullulanase-debranched pea starch by oleic acid complexation

Wenjie Fu[1], Dong Kong[1], Hong Liu[2], Ziyu Zhuang[1], Shanli Peng[1], Jiaojiao Yu[1*], Hui Ji[1*]

1. College of Life Science, Linyi University, Shandong Key Laboratory of Biological Preparation and Application Technology for Functional Glycomics, Linyi, 276005, China.

2. Binzhou Inspection and Testing Center, Binzhou, 256606, China.

[*]Co-corresponding Author: Jiaojiao Yu; Hui Ji

E-mail addresses: yu523198@163.com; hji8002@126.com

Funding

This work was supported by Integration and Demonstration of Key Technologies for Yield Improvement and Value Enhancement of High-Starch Food and Cash Crops for Vermicelli Production (Grant No. X2024TZXD071).

ABSTRACT

Starch-based foods are often rapidly digested, resulting in a high postprandial glycemic response and limiting their application in low-glycemic-index (GI) functional foods. This study aimed to regulate pea starch (PS) digestibility through pullulanase-mediated debranching followed by oleic acid (OA) complexation and to elucidate the underlying structural mechanisms. Appropriate OA addition significantly enhanced the enzymatic resistance of debranched pea starch (DPS), resulting in lower estimated glycemic index (eGI) and higher resistant starch (RS) content. The 6% OA complex exhibited the highest complexation index (CI), lowest eGI (30.91), and highest RS content (55.29%). However, excessive OA addition reduced complexation efficiency and weakened the improvement in starch digestibility. Multi-scale structural characterization showed that appropriate OA addition promoted starch-lipid complex formation, enhanced short-range molecular order and relative crystallinity (RC), generated a more compact microstructure, and improved thermal stability without altering the crystalline polymorph. Pearson correlation analysis further showed that CI, short-range molecular order, and RC were positively correlated with RS but negatively correlated with rapidly digestible starch (RDS) and eGI, indicating that structural ordering and starch-lipid complex formation jointly reduced starch enzymatic accessibility. Overall, this study establishes a structure-digestibility relationship for debranched pea starch-oleic acid (DPS-OA) complexes and provides a feasible strategy for developing low-GI starch-based functional foods.

KEY WORDS: Pea starch; Debranched pea starch-oleic acid complex; In vitro digestibility; Structure

1.Introduction

Driven by shifts in dietary patterns and the rising prevalence of metabolic syndromes-such as diabetes, obesity, and cardiovascular diseases-the development of low-glycemic index (GI) foods has emerged as a critical research focus in food science and nutrition (C.-M. Lee et al., 2025). Starch is the primary source of dietary carbohydrates for humans, and its digestion rate directly influences postprandial blood glucose levels. Rapidly digestible starch (RDS) is rapidly hydrolyzed into glucose during digestion, resulting in a sharp increase in postprandial blood glucose levels (Bello-Perez et al., 2020). In contrast, resistant starch (RS) escapes digestion and absorption in the small intestine and is subsequently fermented by the colonic microbiota. This fermentation process has been associated with multiple physiological benefits, including reduced postprandial glycemic response, modulation of gut microbiota, enhanced production of short-chain fatty acids (SCFAs), and a reduced risk of chronic metabolic diseases(Das et al., 2024). Therefore, increasing the RS content while reducing the GI of starch-based foods has become an important strategy for the development of functional starches.

Pea starch (PS) is widely available, cost-effective, and environmentally friendly. Owing to its excellent gelling properties and high processing stability, it has been extensively utilized in the food industry (L. Gao et al., 2022). Compared with cereal starches such as corn and wheat starch, PS generally contains a higher amylose content of 40-65%, which contributes to the formation of resistant starch and ordered double-helical structures and makes PS a promising ingredient for low-GI foods (Palabiyik et

al., 2017). However, despite its high amylose content, a considerable fraction of PS remains susceptible to enzymatic hydrolysis, and its inherent structural organization limits the further enhancement of digestive resistance. Therefore, further modulation of the molecular structure of PS is required to promote the formation of ordered and enzyme-resistant structures, thereby improving its digestive properties and expanding its potential for low-GI food applications (G. Li et al., 2023).

In recent years, the regulation of starch structure through lipid complexation to reduce starch digestibility has emerged as an important strategy in the development of functional starches. During thermal gelatinization, amylose molecules undergo a conformational transition from random coils to single-helical structures. The hydrophobic cavity of the amylose helix is capable of encapsulating hydrophobic guest molecules, such as fatty acids (FA), leading to the formation of stable starch-lipid inclusion complexes through hydrophobic interactions, hydrogen bonding, and van der Waals forces (S. Wang et al., 2020). The complexation between starch and guest molecules promotes the ordered packing of left-handed single helices, resulting in the formation of a V-type crystalline structure characterized by distinctive X-ray diffraction peaks. This crystalline form has been classified as type V resistant starch (RS5) (J. Chen et al., 2022). Compared with type III resistant starch (RS3) formed through starch retrogradation, the V-type inclusion structure exhibits a more compact molecular packing and superior structural stability. This ordered architecture effectively restricts starch granule swelling and reduces the accessibility of glycosidic linkages to digestive enzymes, thereby slowing starch hydrolysis, increasing RS content, and ultimately

lowering the GI. Increasing evidence has demonstrated that V-type starch-lipid complexes not only improve the crystalline structure and thermal stability of starch but also markedly reduce its in vitro digestibility(S. Sun et al., 2022; S. Zhang et al., 2026). Consequently, they have been widely recognized as an effective strategy for developing low-GI starch-based foods. However, the chain length, degree of unsaturation, and molecular configuration of FA influence their ability to penetrate the amylose helical cavity, thereby determining the complexation efficiency, crystalline characteristics, and digestive behavior of starch-lipid complexes (Hu et al., 2025). Therefore, selecting an appropriate FA is critical for the formation of V-type structures.

Oleic acid (OA), a representative monounsaturated FA, possesses good biocompatibility, nutritional value, and hydrophobicity, making it a potential guest molecule for amylose inclusion complexation (Winfield et al., 2024). Its hydrocarbon chain can interact with the hydrophobic cavity of amylose single helices, facilitating the formation of V-type starch-lipid inclusion complexes. However, the complexation efficiency of FAs is strongly dependent on their molecular structure, particularly chain length, degree of unsaturation, and double-bond configuration (Z. Wang et al., 2026). Compared with saturated FAs, unsaturated FAs generally exhibit lower complexation efficiency, which has been attributed to the steric hindrance and conformational constraints associated with cis double bonds. These structural characteristics may affect the insertion and packing of FA chains within the amylose helical cavity, thereby influencing complex stability, crystalline ordering, and ultimately starch digestibility. Therefore, although OA can form V-type inclusion complexes with amylose, its

structural characteristics should be considered when elucidating the formation and digestive behavior of starch-OA complexes (Seo et al., 2015).

Studies have shown that pullulanase specifically hydrolyzes the α-1,6 glycosidic linkages in amylopectin, converting branched chains into a large number of short linear amylose chains (Hii et al., 2012). The resulting short linear chains exhibit enhanced molecular mobility and can readily rearrange during cooling to form more perfect double-helical structures, thereby improving crystalline order and thermal stability while facilitating the formation of starch-lipid inclusion complexes (Semwal & Meera, 2023). OA can interact with these linear chains to form V-type inclusion complexes, thereby enhancing structural order and resistance to enzymatic hydrolysis (S. Sun et al., 2019). Such inclusion structures may restrict the accessibility of digestive enzymes to starch chains and glycosidic linkages, consequently increasing RS and reducing the glycemic response. Although OA-starch inclusion complexes have been investigated in several starch sources, including corn, potato, and high-amylose starches (Królikowska et al., 2025; Y. Wang et al., 2025), the structural mechanisms underlying the reduced digestibility of debranched pea starch-oleic acid (DPS-OA) complexes remain poorly understood. In particular, how OA-induced complexation and multiscale structural reorganization regulate enzymatic accessibility and ultimately contribute to the reduction of the GI remains to be elucidated.

Against this background, DPS-OA complexes were constructed to elucidate the structural mechanisms underlying their reduced digestibility. Unlike previous studies mainly focusing on starch-FA complex formation or individual structural changes, this

study used DPS as the raw material to construct starch-OA complexes with different concentrations of OA. The complexation behavior, short-range molecular order, crystalline structure, microstructure, and thermal stability were systematically characterized in combination with in vitro digestion properties to elucidate the relationship between multiscale structural reorganization and starch digestibility. The findings provide new insights into the structure-digestibility relationship of starch-lipid complexes and offer a feasible strategy for developing low-GI starch-based functional foods.

2. Materials and methods

2.1 Materials

Pea starch, glucoamylase (100 U/mg), and α-amylase (100 U/mg) were purchased from Yuanye Bio-Technology Co., Ltd. (Shanghai, China). Oleic acid (OA, C18:1) was obtained from Heowns Biochemical Technology Co., Ltd. (Tianjin, China). Pullulanase (EC 3.2.1.41, 1 U/mg) was purchased from Duly Biotechnology Co., Ltd. (Nanjing, China). All other chemicals and reagents used in this study were of analytical grade.

2.2 Preparation of DPS-OA complexes

DPS complexes were prepared with slight modifications to a previously reported method(P. Li et al., 2017). Briefly, pea starch (35 g, dry basis) was dispersed in 0.1 M sodium acetate buffer (pH 4.5) to obtain an 8% (w/v) starch suspension. The suspension was gelatinized by continuous stirring at 95°C for 1 h and then cooled to 55°C. Pullulanase (60 U/g dry starch) was added, and the debranching reaction was performed at 55°C for 12 h. Subsequently, the enzyme was inactivated by heating the mixture at

100°C for 20 min. The resulting suspension was washed three times with anhydrous ethanol and centrifuged at 4000 rpm for 10 min. The washed sample was dried at 40°C, pulverized, and sieved to yield DPS.

Subsequently, 50 mL of a 7% (w/v) DPS suspension was heated at 100°C for 30 min. OA, dissolved in absolute ethanol, was added at concentrations of 1.5%, 3%, 6%, 9%, 12%, and 15% (w/w, based on the dry weight of starch), followed by heating at 100°C for 1 h to promote complex formation (Nie et al., 2024). The mixtures were then cooled to room temperature (25°C), washed three times with absolute ethanol, and centrifuged at 4000 rpm for 10 min after each washing step. The resulting precipitates were dried at 40°C, ground, and passed through an 80-mesh sieve. The obtained DPS-OA complexes were designated as DPS-XOA, where X represents the OA addition level. Accordingly, the samples were labeled as DPS-1.5%OA, DPS-3%OA, DPS-6%OA, DPS-9%OA, DPS-12%OA, and DPS-15%OA.

2.3 Determination of starch hydrolysis rate and estimated glycemic index (eGI) value

The in vitro digestibility of the starch complexes was determined according to the method of (Xu et al., 2020)with slight modifications. Briefly, 400 mg of each sample was dispersed in 10 mL 0.1 M sodium acetate buffer (pH 5.2) and equilibrated in a shaking water bath at 37°C. Subsequently, 1 mL of glucoamylase (120 U/mL) and 1 mL of α-amylase (580 U/mL) were added to initiate enzymatic hydrolysis. Aliquots (0.1 mL) were collected at 0, 20, 40, 60, 80, 100, 120, 150, and 180 min. Each aliquot was immediately mixed with 1 mL of absolute ethanol to terminate enzymatic activity

and centrifuged at 4500 rpm for 10 min. A 0.4 mL portion of the resulting supernatant was thoroughly mixed with 0.3 mL of 3,5-dinitrosalicylic acid (DNS) reagent and heated in a boiling water bath for 5 min. After cooling, the solution was diluted to 5 mL with distilled water, and its absorbance was measured at 540 nm. A glucose standard curve was prepared using glucose standard solutions of different concentrations, and the glucose released at each digestion time was quantified accordingly. The contents of RDS, slowly digestible starch (SDS), and RS were calculated using the following equations:

$$\mathrm{RDS}(\%) = \frac{(G_{20} - G_0) \times 0.9}{C} \times 100$$

$$\mathrm{SDS}(\%) = \frac{(G_{120} - G_{20}) \times 0.9}{C} \times 100$$

$$\mathrm{RS}(\%) = (1 - \mathrm{RDS} - \mathrm{SDS}) \times 100$$

where G0 is the amount of free glucose (mg), G20 and G120 are the amounts of glucose released after 20 and 120 min of enzymatic hydrolysis (mg), respectively, C is the starch content (mg) of the freeze-dried sample and 0.9 is the mass conversion factor for the dehydration of glucose units from glucose to starch.

The hydrolysis index (HI) was calculated as:

$$\mathrm{HI}(\%) = \frac{\mathrm{AUC}_{\mathrm{sample}}}{\mathrm{AUC}_{\mathrm{standard}}} \times 100$$

where $\mathrm{AUC}_{\mathrm{sample}}$ and $\mathrm{AUC}_{\mathrm{standard}}$ represent the area under the hydrolysis curve of the sample and the reference material, respectively.

The eGI was then calculated according to the following equation:

$$\mathrm{eGI} = 0.862 \times \mathrm{HI} + 8.198$$

2.4 Complexing index (CI)

The CI was determined according to a modified method described by (Yan et al., 2022). Briefly, 0.4 g (dry basis) of the DPS-OA complex was accurately weighed and mixed with deionized water to a total mass of 5 g, followed by vortex mixing for 2 min. The suspension was heated in a water bath at 90 °C for 10 min with continuous stirring to ensure complete gelatinization and then cooled to room temperature. Subsequently, 25 mL of deionized water was added, and the mixture was centrifuged at 4000 rpm for 10 min after thorough shaking. An aliquot (0.5 mL) of the supernatant was mixed with 15 mL of deionized water and 1 mL of iodine solution (2.0% KI and 1.3% I_2, w/v) for color development. The absorbance was measured at 690 nm using a UV-Vis spectrophotometer (UV-752N, INESA Analytical Instrument Co., Ltd., Shanghai, China). All measurements were conducted in triplicate. Untreated PS was used as the control. The CI was calculated using the following equation:

$$\mathrm{CI}(\%) = \frac{A_2 - A_1}{A_2} \times 100$$

where A_2 is the absorbance of the untreated PS paste and A_1 is the absorbance of the DPS-OA complex paste.

2.5 Scanning electron microscope (SEM)

PS and the prepared samples were mounted onto aluminum stubs using conductive carbon tape and sputter-coated with a thin layer of gold prior to observation. The surface morphology of the samples was examined using a SEM (EVO 18, Carl Zeiss Management Co., Ltd., Shanghai, China) operated under low-vacuum conditions. The accelerating voltage was set at 15 kV, and the micrographs were acquired with a scale bar of 20 μm (Caihong Wang et al., 2023).

2.6 Fourier transform infrared spectroscopy analysis (FTIR)

FTIR spectra of the DPS-OA complexes were recorded using an FTIR spectrometer (INVENIO S, Bruker Corporation, Germany). The samples were thoroughly mixed with potassium bromide (KBr) powder at a mass ratio of 1:100 and compressed into transparent pellets for analysis (L. Chen et al., 2019). The spectra were collected over the wavenumber range of 4000-400 cm^{-1} with a spectral resolution of 4 cm^{-1}.

2.7 X-ray diffraction (XRD)

The crystalline structure of the samples was characterized using an X-ray diffractometer (DX-2700B, Dandong Haoyuan Instrument Co., Ltd., Dandong, China). XRD patterns were recorded using Cu Kα radiation over a 2θ range of 5°-40° with a step size of 0.05° and a scanning rate of 5°/min (C. Zhang et al., 2022). The RC was calculated according to the following equation:

$$\mathrm{RC}(\%) = \frac{A_a}{A_a + A_b} \times 100$$

Where A_a is the area corresponding to the crystalline region and A_b is the area corresponding to the amorphous region .

2.8 Thermogravimetric analysis (TGA)

The thermal stability of the DPS-OA complexes was evaluated using a thermogravimetric analyzer (HQT-4, Beijing Hengjiu Scientific Instrument Factory, Beijing, China). Approximately 5 mg of each sample was accurately weighed into a ceramic crucible. TGA was performed over the temperature range of 30–650 °C at a heating rate of 20 °C/min. The derivative thermogravimetric (DTG) curves were

obtained from the first derivative of the TGA curves (Thakur, et al., 2023).

2.9 Statistical analysis

Statistical analyses of the DPS-OA complex samples were conducted using SPSS software (Version 25.0, IBM Corp.). All experiments were performed in triplicate, and the results are expressed as mean values. Statistical significance was defined at $P < 0.05$. The data were subjected to one-way analysis of variance (ANOVA), followed by Duncan's multiple range tests to evaluate differences among the means.

3.Results and discussion

3.1 In Vitro Digestibility and eGI of DPS-OA Complexes

To evaluate the effects of different OA concentrations on the digestibility of DPS, the in vitro hydrolysis curves were determined, and the contents of RDS, SDS, RS, and the eGI were calculated. The corresponding results are presented in Fig. 1 and Table 1. The starch hydrolysis rate reflects the rate at which starch is enzymatically converted into glucose. A faster hydrolysis rate is generally associated with a more rapid postprandial increase in blood glucose. As shown in Fig. 1, all samples exhibited rapid hydrolysis during the initial stage of digestion (0-20 min), followed by a gradual decrease in the hydrolysis rate until reaching a relatively stable phase. This behavior is consistent with the typical in vitro digestion characteristics of starch reported previously (Y. Zhang et al., 2025). Nonetheless, manifest variations in the extent of digestion were observed among different samples. PS exhibited the highest hydrolysis rate throughout the digestion process, indicating that the preferential enzymatic degradation of the amorphous regions on the granule surfaces led to accelerated

digestion kinetics. Following pullulanase debranching, the final hydrolysis rate decreased significantly and was substantially lower than that of PS. This result indicates that the abundant short linear amylose chains generated during debranching underwent molecular rearrangement during cooling, forming more stable double-helical and crystalline structures. The resulting increase in RC and structural compactness enhanced the resistance of starch granules to enzymatic hydrolysis (Lu et al.,2018).

The incorporation of OA further reduced the digestion rate of all DPS-OA complexes. Among all samples, the 6% OA complex exhibited the lowest hydrolysis rate throughout the entire digestion process, which was significantly lower than that of the debranched starch and the other OA-treated groups. This finding suggests that an appropriate amount of OA effectively promoted the formation of starch-lipid inclusion complexes (Liu et al., 2024) and upgraded granular structural stability, thereby obstructing the penetration of digestive enzymes into the matrix interior. In contrast, further increasing the OA concentration to 9%, 12%, and 15% resulted in a moderate increase in the final hydrolysis rate, signaling that excessive OA failed to render a further inhibitory effect on digestion and compromised the effective complexation efficiency instead. This phenomenon may be attributed to the limited encapsulation capacity of amylose helical cavities. Once the optimal OA concentration was exceeded, excess OA molecules were unable to enter the amylose helices to form inclusion complexes and instead remained in the system as free molecules or lipid droplets, thereby reducing the overall complexation efficiency. Moreover, excessive OA may interfere with the ordered arrangement of starch chains, partially disrupting crystalline

regions and reducing structural integrity. Consequently, no further improvement in enzymatic resistance was achieved.

As summarized in Table 1, the variations in RDS, SDS, and RS contents were generally consistent with the in vitro digestion profiles. PS exhibited the highest RDS content and the lowest RS content (14.60%), indicating that most starch granules were readily hydrolyzed by α-amylase within a short period, which consequently resulted in a relatively high eGI. Following pullulanase debranching, the RDS content decreased significantly to 31.75%, whereas the RS content increased to 41.60%, indicating that debranching promoted the rearrangement of linear starch chains and enhanced the structural stability of the starch matrix. This finding is in agreement with previous reports (H. Zhang et al., 2024). Upon the incorporation of OA, a further reduction in RDS accompanied by a progressive increase in RS was observed, though this modification did not follow a simple linear relationship. These results indicate that, at an appropriate concentration, OA was efficiently incorporated into the amylose helical cavities to form stable inclusion complexes. This process further enhanced the ordered structure of the starch granules, increased their resistance to enzymatic hydrolysis, and consequently promoted the conversion of RDS into RS (H. Chen et al., 2024). Notably, when the OA concentration exceeded 6%, the RS content decreased slightly and the improvement in eGI became less pronounced, which was consistent with the trend observed in the in vitro digestion curves. These findings further suggest that excessive OA cannot continuously enhance complexation efficiency, indicating the existence of an optimal OA concentration for improving digestion resistance. The changes in the

eGI (Table 2) further confirmed the regulatory effect of OA complexation on starch digestibility. PS exhibited the highest eGI value. After pullulanase debranching, the eGI decreased to 39.19, and a further reduction was observed following OA incorporation. Among all samples, the 6% OA complex exhibited the lowest eGI value of 30.91. The increase in the CI further promoted the formation of a more stable structural barrier surrounding the starch granules, thereby restricting the accessibility of α-amylase to glycosidic linkages. As a result, the samples exhibited a lower eGI, reduced RDS content, and increased RS content. However, when the OA concentration exceeded the optimal level, the improvement in structural stability gradually reached saturation, and no further reduction in eGI was observed (Wu et al., 2025).

3.2 Complex Index (CI) Analysis

The CI was used to evaluate the extent of complex formation between DPS and OA. CI reflects the ability of amylose chains to encapsulate FA through hydrophobic interactions, leading to the formation of amylose-lipid inclusion complexes. A higher CI value indicates a greater degree of starch-lipid complexation and the formation of more stable and ordered V-type inclusion complexes(Tang & Copeland, 2007). The CI values of the DPS-OA complexes are presented in Fig. 2. As shown in Fig. 2, the CI of DPS-OA complexes increased significantly with increasing OA concentration, reached a maximum at 6% OA, and subsequently decreased as the OA content was further increased. The highest CI was observed at an OA addition level of 6%, indicating that the short linear chains generated by pullulanase debranching effectively interacted with OA through helical inclusion structures. This promoted the formation of DPS-OA

inclusion complexes and enhanced their resistance to α-amylase hydrolysis, which was consistent with the in vitro digestion results. The relatively high CI values observed at 6% and 9% OA were consistent with the corresponding RS contents. However, the CI began to decline beyond 9% OA addition, which could be attributed to the accumulation of free FA and the disruption of the ordered alignment of starch chains, suggesting that excess FA predominantly existed in an uncomplexed form (H.-S. Lee et al., 2020). Previous studies have demonstrated that an appropriate amount of OA facilitates the formation of V-type amylose-lipid inclusion complexes, whereas excessive FA addition decreases the complexation efficiency because of the accumulation of free FA (Zhou et al.,2022). Although the CI exhibited a slight increase at an OA concentration of 15%, it remained lower than that of the optimal group. In addition, the retrogradation of amylose during the cooling process may also contribute to the observed changes in CI. This phenomenon may be attributed to the limited interaction between debranched starch chains and OA at excessive lipid levels, which is consistent with previous observations (S. Sun et al., 2019). Collectively, these results indicate that an appropriate OA concentration effectively promotes the formation of starch-lipid inclusion complexes(Zheng et al., 2020).

3.3 Microscopic structure of complexes

The morphological changes of PS, DPS, and DPS-OA complexes are presented in Fig. 3. As shown in Fig. 3a, PS exhibited intact oval granules with smooth surfaces and well-defined boundaries. After pullulanase debranching (Fig. 3b), the original granular architecture was completely disrupted and transformed into irregular compact

aggregates and sheet-like rearranged structures. This structural transition can be attributed to the hydrolysis of α-1,6 glycosidic linkages in amylopectin by pullulanase, which induced the collapse of the crystalline regions and the disordered retrogradation of short linear starch chains, consistent with previous reports (Z. Wang et al., 2026). Following complexation with OA and subsequent drying, the DPS-OA complexes exhibited distinct particulate structures superimposed on the original sheet-like morphology of DPS, indicating the successful formation of starch-lipid complexes. At low OA addition levels (1.5-3%, Fig. 3c-d), the surface roughness of the samples increased, while some large aggregated structures characteristic of debranched starch remained, suggesting that complex formation was still incomplete. As the OA concentration increased to 6%-9% (Fig. 3e-f), the bulky structures dissipated and converted into highly fragmented, uniformly sized micro-granular aggregates. This observation suggests that strong self-assembly occurred between OA molecules and short linear starch chains, leading to the formation of a dense and homogeneous V-type inclusion complex network (X. Sun et al., 2025). Such a compact microstructure is expected to hinder enzyme accessibility and thereby retard starch hydrolysis. These morphological changes were in good agreement with the CI results discussed above, further confirming the enhanced starch-lipid complexation at the optimal OA concentration. However, when the OA content was further increased to 12-15% (Fig. 3g-h), excess free OA accumulated on the surface of the complexes. The enhanced hydrophobic interactions together with steric hindrance promoted secondary aggregation of the particles, resulting in larger aggregates with blurred particle

boundaries.

3.4 Fourier Transform Infrared (FTIR) Spectroscopy Analysis

FTIR spectroscopy was employed to qualitatively investigate the changes in functional groups, intermolecular interactions, and structural characteristics during the complexation of DPS with OA by analyzing the positions and intensities of characteristic absorption bands (Chi et al., 2017). The FTIR spectra of PS, DPS, and DPS-OA complexes are presented in Fig. 4. Compared with NPS, no novel absorption peaks emerged in DPS, demonstrating that enzymatic debranching did not alter the fundamental chemical backbone of the starch. The broad absorption band centered at approximately 3400 cm^{-1} was assigned to the O-H stretching vibration (Xiong et al., 2017). After debranching and OA incorporation, the intensity of this band gradually decreased and exhibited a slight red shift, indicating the formation of stronger hydrogen-bonding interactions between the hydroxyl groups of starch chains and the carboxyl groups of OA. These interactions enhanced intermolecular association and contributed to the stabilization of the starch-lipid inclusion complexes. After the addition of OA, two distinct absorption bands appeared at 2925 cm^{-1} and 2854 cm^{-1}, corresponding to the asymmetric and symmetric stretching vibrations of the methyl and methylene groups in the aliphatic chains of OA, respectively (Shujun Wang et al.,2016). The intensities of these characteristic bands gradually increased with increasing OA concentration. Although the carbonyl (C=O) stretching vibration of free FA is typically observed near 1700 cm^{-1}, this absorption band was not clearly detectable in the spectra of the DPS-OA complexes. This observation aligns with the findings reported by Ma et

al. (2026) at 1700 cm^{-1}. This phenomenon may be attributed to hydrogen bonding between the carboxyl groups of OA and the hydroxyl groups of starch, with OA molecules being encapsulated within the helical cavities of amylose in the form of inclusion complexes. Consequently, the characteristic carbonyl peak of OA was substantially attenuated or masked due to hydrogen bonding and host-guest encapsulation effects.

The intensity ratio of the absorption bands at 1047 and 1022 cm^{-1} is widely used as an indicator of the short-range molecular order of starch (Shujun Wang et al.,2016). As summarized in Table 2, PS exhibited the lowest 1047/1022 ratio (1.001), which increased to 1.008 after pullulanase debranching, suggesting that the short linear amylose chains generated by debranching rearranged more readily, thereby enhancing localized structural order. Upon OA incorporation, the 1047/1022 ratio increased further and reached a maximum value of 1.040 at an OA concentration of 6%. A slight decrease was observed at 9% OA (1.038), followed by a more pronounced reduction to 1.010 and 1.001 at 12% and 15% OA, respectively. These results indicate that an appropriate amount of OA promoted the formation of more stable amylose-lipid inclusion complexes, thereby improving the short-range molecular order of the starch structure (S. Sun et al., 2021). However, when the OA concentration exceeded the optimal level, the available amylose chains capable of forming inclusion complexes gradually became saturated. Consequently, excess OA was unable to enter the amylose helical cavities and instead remained in free or aggregated forms, thereby diminishing its ability to promote the formation of ordered structures. These spectral data exhibit a

strong correlation with the RC results.

3.5 X-ray Diffraction (XRD) Analysis

The XRD patterns and RC values of PS, DPS, and DPS-OA complexes are presented in Fig. 5 and Table 2, respectively. PS exhibited characteristic diffraction peaks at approximately 15°, 17°, and 23° (2θ), corresponding to the typical C-type crystalline pattern (Z. Ma et al., 2018). Following pullulanase debranching, the α-1,6 glycosidic linkages of amylopectin were selectively hydrolyzed, generating abundant short linear starch chains with enhanced molecular mobility and a greater tendency to undergo molecular rearrangement. During retrogradation, these short linear chains were closely associated through hydrogen bonding to form double-helical structures, resulting in markedly enhanced B-type diffraction peaks at approximately 17° and 22°. Consequently, the debranched sample achieved the highest RC of 18.94%. This observation is consistent with previous studies reporting that debranched starch preferentially forms B-type crystalline structures during molecular reassociation (Van Hung et al., 2012; Zeng et al., 2015). Although OA was incorporated after pullulanase debranching, no obvious crystalline polymorphic transition was observed in the XRD patterns. This phenomenon may be attributed to the predominance of the recrystallized starch phase formed during debranching, whereas only a portion of the amylose chains participated in inclusion complex formation with OA. Consequently, the proportion of newly formed V-type inclusion crystallites was insufficient to alter the overall crystalline polymorph of the starch system. In addition, the cis double bond in OA introduced steric hindrance, resulting in a less ordered arrangement of the inclusion

complexes compared with those formed using saturated FA. Therefore, although the overall crystalline polymorph remained unchanged, the locally formed inclusion complexes effectively restricted enzyme accessibility, thereby increasing the RS content and reducing the eGI.

Among the OA-treated samples, the RC initially increased with increasing OA concentration and then gradually reached a plateau. At an OA concentration of 1.5%, the RC decreased to 14.51%, probably because the limited amount of OA was insufficient to effectively interact with the pre-existing crystalline regions. Increasing the OA concentration to 6% significantly increased the RC to 17.65%, the highest value among the OA-treated samples, accompanied by a more pronounced V-type characteristic diffraction peak (Q. Gao et al., 2024). These results suggest that an OA concentration of 6% was optimal for promoting the formation of highly ordered inclusion structures under the present experimental conditions. However, when the OA concentration was further increased to 9-15%, the RC no longer increased but instead showed a slight decline (S. Sun et al., 2019). This decrease was mainly attributed to the saturation of available complexation sites. Excess OA molecules remained outside the crystalline domains because the amount of amylose available for inclusion complex formation had become limiting. These uncomplexed OA molecules interfered with further crystal growth and reduced the structural order of the complexes. Notably, RC was not completely positively correlated with digestion resistance. Although DPS exhibited the highest RC, its RS content was lower than that of the 6% OA complex. These findings indicate that starch digestibility is governed not only by the degree of

crystallinity but also by multiple structural factors, including the CI, short-range molecular order, and RS content (Q. Ma, Jia, et al., 2026). Therefore, the V-type inclusion structures formed at an appropriate OA concentration further restricted enzyme penetration into the starch matrix. Consequently, despite exhibiting a slightly lower overall crystallinity than DPS, the 6% OA complex displayed superior digestion resistance and a lower eGI.

3.6 Thermogravimetric Analysis (TGA)

Thermogravimetric (TG) and DTG analyses were performed to evaluate the thermal degradation behavior and thermal stability of PS, DPS, and DPS-OA complexes. The corresponding TG (a) and DTG (b) curves are presented in Fig. 6. All samples exhibited three characteristic weight-loss stages, which are consistent with previous reports (Marinopoulou et al., 2016). The first stage (50-150°C) was mainly associated with the evaporation of free and bound water. The second stage (approximately 280-360°C) corresponded to the primary thermal degradation of starch, during which glycosidic bond cleavage, molecular depolymerization, and the release of volatile oligosaccharides resulted in rapid mass loss. The third stage (approximately 400-520°C) was mainly attributed to the further thermal decomposition of residual carbonaceous structures and starch-lipid complexes. As shown by the DTG (b) curves, all samples exhibited a pronounced maximum degradation rate peak at approximately 320-330°C, corresponding to the rapid thermal decomposition of the starch backbone. Compared with PS, DPS exhibited a markedly lower maximum degradation rate and the highest char residue at 600°C among all samples, indicating that pullulanase

debranching significantly enhanced the thermal stability of the starch system (Thakur et al., 2023). Combined with the XRD results, this behavior can be explained by the selective hydrolysis of amylopectin branches by pullulanase, which generated abundant short linear starch chains. During cooling and retrogradation, these chains readily rearranged into ordered double-helical structures, resulting in higher RC. The enhanced structural order strengthened intermolecular interactions and increased the resistance of starch chains to thermal degradation, thereby reducing the degradation rate and increasing the final char residue. These findings indicate that pullulanase debranching not only promoted the reconstruction of the starch crystalline structure but also improved its thermal stability, which is in good agreement with the increased RC observed by XRD.

Compared with DPS, the incorporation of OA caused noticeable changes in both the TG and DTG curves. The most prominent feature was the appearance of a new DTG (b) degradation peak at approximately 480-490°C, which was absent in both PS and DPS, indicating that OA altered the thermal degradation behavior of the system during the later stages of heating (Di Marco et al., 2020). This specific degradation peak may be ascribed to the high-temperature pyrolytic decomposition of OA encapsulated within the single-helical cavities of amylose, alongside a minor fraction of uncomplexed OA. Concurrently, the final char residue of all DPS-OA complexes were lower than that of DPS, primarily because OA predominantly undergoes thermal cracking to generate volatile products at elevated temperatures, thereby reducing the final solid residue. The thermal stability of the complexes was strongly influenced by the OA concentration. As

the OA concentration increased, the char residue initially increased, then decreased, and finally showed a slight recovery at the highest OA level. Among the OA-treated samples, the 6% OA complex exhibited a relatively high char residue, suggesting that an appropriate amount of OA promoted the formation of stable starch-lipid inclusion complexes, thereby enhancing the overall thermal stability of the system (Q. Gao et al., 2024). When the OA concentration was further increased to 15%, the char residue exhibited a slight increase. It is hypothesized that a portion of the excess OA, failing to participate in complexation, accumulated on the surface of the starch granules. During pyrolysis, these surface-associated OA molecules may have partially hindered heat transfer, thereby slowing further thermal degradation and resulting in a slightly higher residual mass.

3.7 Relationship between multi-scale structural characteristics and digestibility of DPS-OA complexes

To further elucidate the intrinsic relationship between starch structural characteristics and digestive behavior, Pearson correlation analysis was performed among the short-range molecular order (1047/1022), CI, RC, eGI, RDS, SDS, and RS. The results are presented in Fig. 7. In the correlation matrix, red and blue represent positive and negative correlations, respectively, while darker colors indicate stronger correlations. The correlation coefficient (r) ranges from −1 to 1. As shown in Fig. 7, significant correlations were observed between the structural parameters of starch and its digestive properties. First, the1047/1022 ratio exhibited highly significant positive correlations with RC ($r = 0.92$, $p < 0.01$) and RS ($r = 0.91$, $p < 0.01$). This finding is

consistent with the results reported by Sun et al. (2024), indicating that the short-range ordered structure characterized by FTIR is well aligned with the long-range crystalline structure determined by XRD (R. Sun et al., 2024). Together, these structural features promoted the formation of RS. These results suggest that a more ordered molecular arrangement facilitated the formation of stable crystalline domains within starch granules, thereby effectively reducing the accessibility of α-amylase to glycosidic linkages. RC exhibited a significant positive correlation with RS ($r = 0.89$, $p < 0.01$) but negative correlations with eGI ($r = -0.86$, $p < 0.01$). This further substantiates that an increase in RC contributes to reducing the proportion of the rapidly digestible fraction and elevating the RS content, ultimately slowing down the digestion rate and lowering the eGI. These findings are consistent with the XRD and in vitro digestion results discussed above, indicating that the development of ordered crystalline structures is one of the key factors responsible for improving starch digestion resistance. The CI was positively correlated with the 1047/1022 ratio, RC, and RS, whereas negative correlations were observed with eGI and RDS.

These results indicate that enhanced starch-OA complexation promoted the development of more ordered internal structures within the starch granules, thereby increasing their resistance to enzymatic hydrolysis (Cuiping Wang et al., 2024). Although the correlation between CI and RC was slightly weaker than that between the 1047/1022 ratio and RC, the results nevertheless demonstrate that inclusion complexation is an important driving force for improving structural ordering in starch. In addition, RS was negatively correlated with RDS ($r = -0.79$, $p < 0.05$), indicating

552 that an increase in RS effectively reduced the proportion of RDS slowed glucose release,
553 and consequently lowered the eGI. These findings further confirm that RS is an
554 important indicator for evaluating starch digestibility. In conclusion, synthesizing the
555 Pearson correlation analysis alongside FTIR, XRD, CI, and in vitro digestion results,
556 demonstrates that the formation of stable starch-lipid inclusion complexes between OA
557 and DPS simultaneously enhanced both the short-range molecular order and the long-
558 range crystalline structure while increasing the degree of complexation. These
559 structural modifications improved the overall stability of the starch granules, restricted
560 the diffusion of digestive enzymes into the granule interior and their access to
561 glycosidic linkages, ultimately resulting in reduced RDS and eGI values together with
562 an increased RS content. These insights further corroborate that the enhancement of
563 starch structural ordering constitutes the primary structural basis by which OA
564 improves the digestive properties of DPS.

565 **Conclusion**

566 This study systematically elucidated the role of OA concentration in regulating the
567 structural characteristics and digestive behavior of DPS. Pullulanase debranching
568 generated short linear glucan chains that favored starch-lipid inclusion complex
569 formation, while OA further promoted a more ordered and compact starch structure.
570 OA enhanced molecular ordering and RC without altering the crystalline polymorph,
571 accompanied by improved thermal stability. However, this effect was concentration-
572 dependent, and excessive OA reduced complexation efficiency as the inclusion capacity
573 of amylose helices became saturated. Among all treatments, the 6% OA complex

showed the most balanced structural and functional properties, with the highest CI, enhanced structural order, increased RS content, and lowest eGI. These results indicate that appropriate starch-lipid complexation, rather than simply increasing FA content, is more effective for improving starch nutritional quality. Pearson correlation analysis further linked short-range molecular order, RC, and complexation degree with starch digestibility, suggesting that enhanced structural ordering plays a key role in increasing enzymatic resistance and reducing starch digestibility. Overall, this study provides insights into the structure-digestibility relationship of DPS-OA complexes and their potential for developing low-GI functional foods. however, the simplified in vitro digestion model and limited molecular-level evidence warrant further validation using physiologically relevant digestion systems and advanced molecular characterization to clarify the underlying mechanisms and facilitate practical food applications.

CRediT authorship contribution statement

Wen-jie Fu: Writing-review & editing, Funding acquisition, Visualization; Dong Kong: Formal analysis, Investigation; Hong Liu: Investigation; Zi-yu Zhuang: Data curation; Shan-li Peng: Funding acquisition; Jiao-jiao Yu: Investigation, Formal analysis; Hui Ji: Methodology, Conceptualization.

Declaration of Competing Interest

The authors declare that they have no known competing financial interests or personal relationships that could have appeared to influence the work reported in this paper.

Data availability

Data will be made available on request.

References

Bello-Perez, L. A., Flores-Silva, P. C., Agama-Acevedo, E., & Tovar, J. (2020). Starch digestibility: past, present, and future. *Journal of the Science of Food and Agriculture, 100*(14), 5009-5016. doi:https://doi.org/10.1002/jsfa.8955

Chen, H., Wang, X., Jin, D., Wu, X., Fang, Y., Lin, Q., & Ding, Y. (2024). Interactions between pectin, starch and linoleic acid and their effects on starch structure, digestion and release properties. *International Journal of Biological Macromolecules, 275*, 133255. doi:https://doi.org/10.1016/j.ijbiomac.2024.133255

Chen, J., Cai, H., Yang, S., Zhang, M., Wang, J., & Chen, Z. (2022). The formation of starch-lipid complexes in instant rice noodles incorporated with different fatty acids: Effect on the structure, in vitro enzymatic digestibility and retrogradation properties during storage. *Food Res Int, 162*(Pt A), 111933. doi:10.1016/j.foodres.2022.111933

Chen, L., McClements, D. J., Zhang, H., Zhang, Z., Jin, Z., & Tian, Y. (2019). Impact of amylose content on structural changes and oil absorption of fried maize starches. *Food Chemistry, 287*, 28-37. doi:https://doi.org/10.1016/j.foodchem.2019.02.083

Chi, C., Li, X., Zhang, Y., Chen, L., Li, L., & Wang, Z. (2017). Digestibility and supramolecular structural changes of maize starch by non-covalent interactions with gallic acid. *Food & Function, 8*(2), 720-730. doi:10.1039/c6fo01468b

Das, M., Santra, S., Chakraborty, M., Rajan, N., Sarvanabhupathy, S., Anusha, et al. (2024). Resistant starch: Insights into better health and metabolism. *Biocatalysis and Agricultural Biotechnology, 59*, 103275.

618 doi:https://doi.org/10.1016/j.bcab.2024.103275
619 Di Marco, A. E., Ixtaina, V. Y., & Tomás, M. C. (2020). Inclusion complexes of high
620 amylose corn starch with essential fatty acids from chia seed oil as potential delivery
621 systems in food. *Food Hydrocolloids, 108*, 106030.
622 doi:https://doi.org/10.1016/j.foodhyd.2020.106030
623 Gao, L., Wu, Y., Wan, C., Wang, P., Yang, P., Gao, X., et al. (2022). Structural and
624 physicochemical properties of pea starch affected by germination treatment. *Food*
625 *Hydrocolloids, 124*, 107303. doi:https://doi.org/10.1016/j.foodhyd.2021.107303
626 Gao, Q., Feng, R., Yu, M.-J., Tao, H., & Zhang, B. (2024). Oleic acid treatment of rice
627 grains reduces the starch digestibility: Formation, binding state and fine structure of
628 starch-lipid complexes. *Food Chemistry, 457*, 140191.
629 doi:https://doi.org/10.1016/j.foodchem.2024.140191
630 Hii, S. L., Tan, J. S., Ling, T. C., & Ariff, A. B. (2012). Pullulanase: role in starch
631 hydrolysis and potential industrial applications. *Enzyme Res, 2012*, 921362.
632 doi:10.1155/2012/921362
633 Hu, W.-X., Dang, Y.-Y., Fu, J.-Y., Jin, C.-S., Li, S.-L., Yu, X., & Du, S.-k. (2025). Effect
634 of fatty acid chain length on the structure and digestibility of high-amylose starch-fatty
635 acid and high-amylose starch-fatty acid-whey protein isolate complexes. *International*
636 *Journal of Biological Macromolecules, 308*, 142616.
637 doi:https://doi.org/10.1016/j.ijbiomac.2025.142616
638 Królikowska, K., Pająk, P., Pietrzyk, S., Czaplak, K., & Strządała, K. (2025).
639 Comprehensive Evaluation of OS Starch–Oleic Acid Mixtures: From Functional

Properties to Their Application in Films with Improved Water Resistance. *Molecules, 30*(22), 4411. doi:10.3390/molecules30224411

Lee, C.-M., Jeong, O.-Y., Park, H.-S., Seo, J., Park, S., Lee, K.-M., et al. (2025). Evaluation of glycemic response and starch digestibility in Korean rice toward the development of low GI rice. *Frontiers in Plant Science, Volume 16 - 2025*. doi:10.3389/fpls.2025.1724565

Lee, H.-S., Kim, K.-H., Park, S.-H., Hur, S.-W., & Auh, J.-H. (2020). Amylose-Lipid Complex as a Fat Replacement in the Preparation of Low-Fat White Pan Bread. *Foods, 9*(2), 194. doi:10.3390/foods9020194

Li, G., Ge, X., Guo, C., & Liu, B. (2023). Effect of Ultrasonic Treatment on Structure and Physicochemical Properties of Pea Starch. *Foods, 12*(13), 2620. doi:10.3390/foods12132620

Li, P., He, X., Dhital, S., Zhang, B., & Huang, Q. (2017). Structural and physicochemical properties of granular starches after treatment with debranching enzyme. *Carbohydrate Polymers, 169*, 351-356. doi:https://doi.org/10.1016/j.carbpol.2017.04.036

Liu, H., Meng, P., Zhang, Y., Zheng, B., & Zeng, H. (2024). Complexation of V-type lotus seed starch and butyric acid: Structure and in vitro digestion. *Food Hydrocolloids, 149*, 109527. doi:https://doi.org/10.1016/j.foodhyd.2023.109527

Lu, Z.-H., Belanger, N., Donner, E., & Liu, Q. (2018). Debranching of pea starch using pullulanase and ultrasonication synergistically to enhance slowly digestible and resistant starch. *Food Chemistry, 268*, 533-541.

doi:https://doi.org/10.1016/j.foodchem.2018.06.115

Ma, Q., Jia, S., Yan, S., Liu, S., Wang, X., Hu, Y., et al. (2026). Structural insights into fatty acid-driven enhancement of digestive resistance in high-amylose maize starch-lipid complexes. *International Journal of Biological Macromolecules, 371*, 152882. doi:https://doi.org/10.1016/j.ijbiomac.2026.152882

Ma, Q., Zang, Z., Yan, S., Han, B., Liu, S., Wang, X., et al. (2026). Structural Reconstruction and Enhanced Digestive Resistance in High-Amylose Maize Starch–Fatty Acid Complexes via Debranching and Heat–Moisture Treatment. *Foods, 15*(5), 907. doi:10.3390/foods15050907

Ma, Z., Yin, X., Chang, D., Hu, X., & Boye, J. I. (2018). Long- and short-range structural characteristics of pea starch modified by autoclaving, α-amylolysis, and pullulanase debranching. *International Journal of Biological Macromolecules, 120*, 650-656. doi:https://doi.org/10.1016/j.ijbiomac.2018.08.132

Marinopoulou, A., Papastergiadis, E., & Raphaelides, S. N. (2016). An investigation into the structure, morphology and thermal properties of amylomaize starch-fatty acid complexes prepared at different temperatures. *Food Research International, 90*, 111-120. doi:https://doi.org/10.1016/j.foodres.2016.10.035

Nie, M., Li, J., Lin, R., Gong, X., Dang, B., Zhang, W., et al. (2024). The role of C18 fatty acids in improving the digestion and retrogradation properties of highland barley starch. *Food Res Int, 186*, 114355. doi:10.1016/j.foodres.2024.114355

Palabiyik, İ., Toker, O. S., Karaman, S., & Yildiz, Ö. (2017). A modeling approach in the interpretation of starch pasting properties. *Journal of Cereal Science, 74*, 272-278.

684 doi:https://doi.org/10.1016/j.jcs.2017.02.008
685 Semwal, J., & Meera, M. S. (2023). Modification of sorghum starch as a function of
686 pullulanase hydrolysis and infrared treatment. *Food Chemistry, 416*, 135815.
687 doi:https://doi.org/10.1016/j.foodchem.2023.135815
688 Seo, T.-R., Kim, J.-Y., & Lim, S.-T. (2015). Preparation and characterization of
689 crystalline complexes between amylose and C18 fatty acids. *LWT - Food Science and*
690 *Technology, 64*(2), 889-897. doi:https://doi.org/10.1016/j.lwt.2015.06.021
691 Sun, R., Chao, C., Wang, C., Yu, J., Copeland, L., & Wang, S. (2024). Key structural
692 factors that determine the in vitro enzymatic digestibility of amylose-complexes.
693 *Carbohydrate Polymers, 342*, 122383.
694 doi:https://doi.org/10.1016/j.carbpol.2024.122383
695 Sun, S., Hong, Y., Gu, Z., Cheng, L., Li, Z., & Li, C. (2019). An investigation into the
696 structure and digestibility of starch-oleic acid complexes prepared under various
697 complexing temperatures. *International Journal of Biological Macromolecules, 138*,
698 966-974. doi:https://doi.org/10.1016/j.ijbiomac.2019.07.166
699 Sun, S., Hua, S., Hong, Y., Gu, Z., Cheng, L., Ban, X., et al. (2022). Influence of
700 different kinds of fatty acids on the behavior, structure and digestibility of high amylose
701 maize starch–fatty acid complexes. *Journal of the Science of Food and Agriculture,*
702 *102*(13), 5837-5848. doi:https://doi.org/10.1002/jsfa.11933
703 Sun, S., Jin, Y., Hong, Y., Gu, Z., Cheng, L., Li, Z., & Li, C. (2021). Effects of fatty
704 acids with various chain lengths and degrees of unsaturation on the structure,
705 physicochemical properties and digestibility of maize starch-fatty acid complexes.

Food Hydrocolloids, 110, 106224. doi:https://doi.org/10.1016/j.foodhyd.2020.106224

Sun, X., Jin, R., Ma, F., Ma, W., Pan, Y., Liu, J., et al. (2025). Effects of different fatty acids on the structure, physicochemical properties, and in vitro digestibility of Chinese yam resistant starch-lipid complexes. *Food Chemistry, 465*, 142159. doi:https://doi.org/10.1016/j.foodchem.2024.142159

Tang, M. C., & Copeland, L. (2007). Analysis of complexes between lipids and wheat starch. *Carbohydrate Polymers, 67*(1), 80-85. doi:https://doi.org/10.1016/j.carbpol.2006.04.016

Thakur, M., Rai, A. K., & Singh, S. P. (2023). Structural Characteristics, Physicochemical Properties, and Digestibility Analysis of Resistant Starch Type-V Prepared from Debranched Corn Starch and Fatty Acid Complexation. *ACS Omega, 8*(29), 25799-25807. doi:10.1021/acsomega.3c01093

Van Hung, P., Lan Phi, N. T., & Vy Vy, T. T. (2012). Effect of debranching and storage condition on crystallinity and functional properties of cassava and potato starches. *Starch - Stärke, 64*(12), 964-971. doi:https://doi.org/10.1002/star.201200039

Wang, C., Chao, C., Sun, R., Yu, J., Copeland, L., & Wang, S. (2024). Structural Factors That Determine the Amylolytic Properties of Starch–Lipid Complexes. *Journal of Agricultural and Food Chemistry, 72*(24), 13918-13928. doi:10.1021/acs.jafc.4c02260

Wang, C., Zhu, Z., Mei, L., Xia, Y., Chen, X., Mustafa, S., & Du, X. (2023). The structural properties and resistant digestibility of maize starch-glyceride monostearate complexes. *International Journal of Biological Macromolecules, 249*, 126141. doi:https://doi.org/10.1016/j.ijbiomac.2023.126141

Wang, S., Chao, C., Cai, J., Niu, B., Copeland, L., & Wang, S. (2020). Starch-lipid and starch-lipid-protein complexes: A comprehensive review. *Compr Rev Food Sci Food Saf, 19*(3), 1056-1079. doi:10.1111/1541-4337.12550

Wang, S., Wang, J., Yu, J., & Wang, S. (2016). Effect of fatty acids on functional properties of normal wheat and waxy wheat starches: A structural basis. *Food Chemistry, 190*, 285-292. doi:https://doi.org/10.1016/j.foodchem.2015.05.086

Wang, S., Zhang, X., Wang, S., & Copeland, L. (2016). Changes of multi-scale structure during mimicked DSC heating reveal the nature of starch gelatinization. *Scientific Reports, 6*(1), 28271. doi:10.1038/srep28271

Wang, Y., Liu, T., Han, T., Xie, J., Sun, L., Zhang, S., et al. (2025). Construction and characterization of novel starch-oleic acid conjugates catalyzed by microwave-assisted lipase reaction. *International Journal of Biological Macromolecules, 306*, 141507. doi:https://doi.org/10.1016/j.ijbiomac.2025.141507

Wang, Z., Liu, Y., Gao, R., Chen, R., Wu, Y., & Ouyang, J. (2026). Impact of amylose, fatty acid chain length and unsaturation on the structural and digestive properties of maize starch–lipid complexes. *International Journal of Biological Macromolecules, 357*, 151645. doi:https://doi.org/10.1016/j.ijbiomac.2026.151645

Winfield, D. D., Dunn, R. O., Winkler-Moser, J. K., Cermak, S. C., & Marks, D. M. (2024). Characterization, physical properties, and potential industrial applications of high oleic pennycress oil. *Industrial Crops and Products, 210*, 118095. doi:https://doi.org/10.1016/j.indcrop.2024.118095

Wu, M., Wu, C., Wang, Y., Bian, X., Liang, D., Zhang, G., et al. (2025). Correlation

between gastrointestinal index (GI) and the structure and physicochemical properties of rice starch from different varieties and colors. *Carbohydrate Polymer Technologies and Applications, 9*, 100687. doi:https://doi.org/10.1016/j.carpta.2025.100687

Xiong, J., Li, Q., Shi, Z., & Ye, J. (2017). Interactions between wheat starch and cellulose derivatives in short-term retrogradation: Rheology and FTIR study. *Food Research International, 100*, 858-863. doi:https://doi.org/10.1016/j.foodres.2017.07.061

Xu, H., Zhou, J., Yu, J., Wang, S., Copeland, L., & Wang, S. (2020). Revealing the mechanisms of starch amylolysis affected by tea catechins using surface plasmon resonance. *International Journal of Biological Macromolecules, 145*, 527-534. doi:https://doi.org/10.1016/j.ijbiomac.2019.12.161

Yan, Z., Zhang, M., Xu, M., Yu, J., Copeland, L., Huang, Y., & Wang, S. (2022). Effect of Debranching and Differential Ethanol Precipitation on the Formation and Fermentation Properties of Maize Starch–Lipid Complexes. *Journal of Agricultural and Food Chemistry, 70*(29), 9132-9142. doi:10.1021/acs.jafc.2c03081

Zeng, S., Wu, X., Lin, S., Zeng, H., Lu, X., Zhang, Y., & Zheng, B. (2015). Structural characteristics and physicochemical properties of lotus seed resistant starch prepared by different methods. *Food Chemistry, 186*, 213-222. doi:https://doi.org/10.1016/j.foodchem.2015.03.143

Zhang, C., Narayanamoorthy, S., Ming, S., Li, K., Cantre, D., Sui, Z., & Corke, H. (2022). Rheological properties, structure and digestibility of starches isolated from common bean (Phaseolus vulgaris L.) varieties from Europe and Asia. *LWT, 161*,

113352. doi:https://doi.org/10.1016/j.lwt.2022.113352

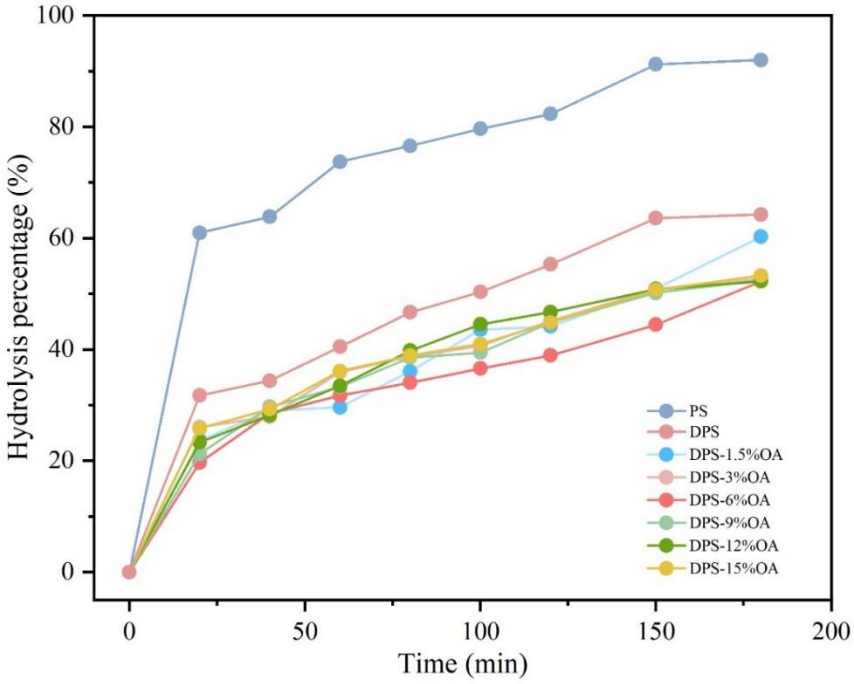
Zhang, H., Sun, S., Cheng, L., Li, Z., Li, C., Hong, Y., & Gu, Z. (2024). Effects of heat moisture treatment on the structure and digestibility of high amylose starch-lauric acid complexes. *Food Hydrocolloids, 151*, 109803. doi:https://doi.org/10.1016/j.foodhyd.2024.109803

Zhang, S., Zhang, X., Liu, J., Yang, J., Xu, X., Tian, H., et al. (2026). Effect of fatty acid chain length and assembly sequence on the structure and digestibility of wheat starch-β-lactoglobulin-fatty acids ternary complexes. *Food Research International, 231*, 118805. doi:https://doi.org/10.1016/j.foodres.2026.118805

Zhang, Y., Wang, C., Chao, C., Yu, J., Yang, Y., & Wang, S. (2025). Effect of debranching on the formation and in vitro digestibility of high amylose maize starch-C18 unsaturated fatty acid complexes. *Carbohydrate Polymers, 357*, 123445. doi:https://doi.org/10.1016/j.carbpol.2025.123445

Zheng, Y., Ou, Y., Zhang, Y., Zheng, B., Zeng, S., & Zeng, H. (2020). Effects of pullulanase pretreatment on the structural properties and digestibility of lotus seed starch-glycerin monostearin complexes. *Carbohydrate Polymers, 240*, 116324. doi:https://doi.org/10.1016/j.carbpol.2020.116324

Zhou, J., Guo, J., Gladden, I., Contreras, A., & Kong, L. (2022). Complexation ability and physicochemical properties of starch inclusion complexes with C18 fatty acids. *Food Hydrocolloids, 123*, 107175. doi:https://doi.org/10.1016/j.foodhyd.2021.107175



793

794 Fig. 1. In vitro starch hydrolysis profiles of PS, DPS, and DPS-OA complexes.

795

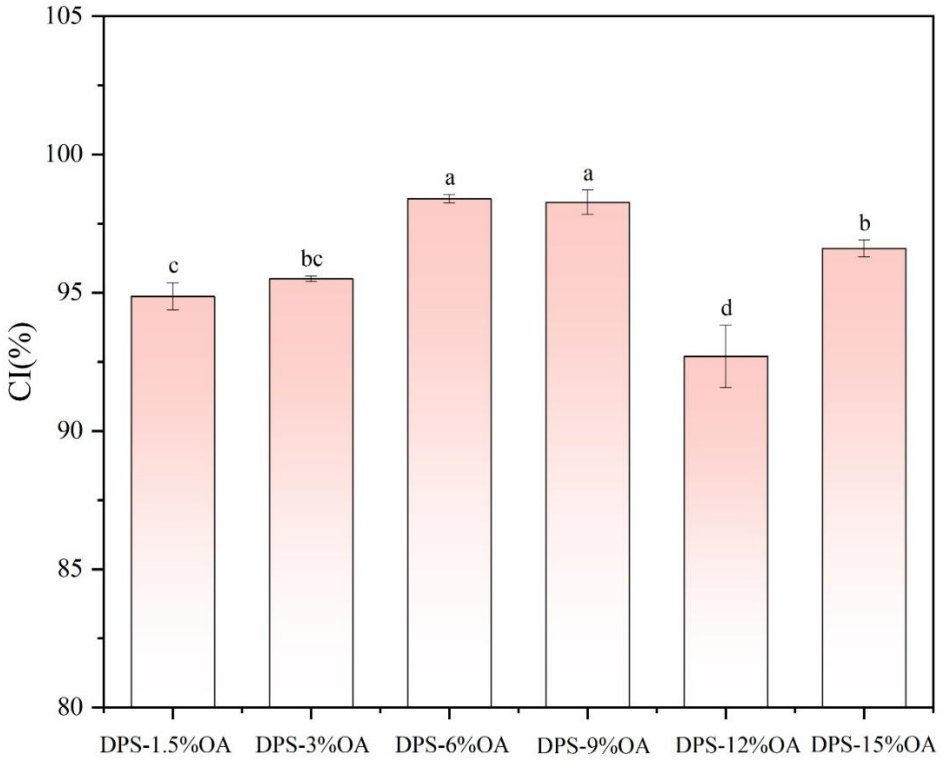


Fig. 2. Effect of OA concentration on the CI of DPS-OA complexes. Results are expressed as Means ± standard deviations (n=3). Means followed by different letters indicate statistical difference (P<0.05).

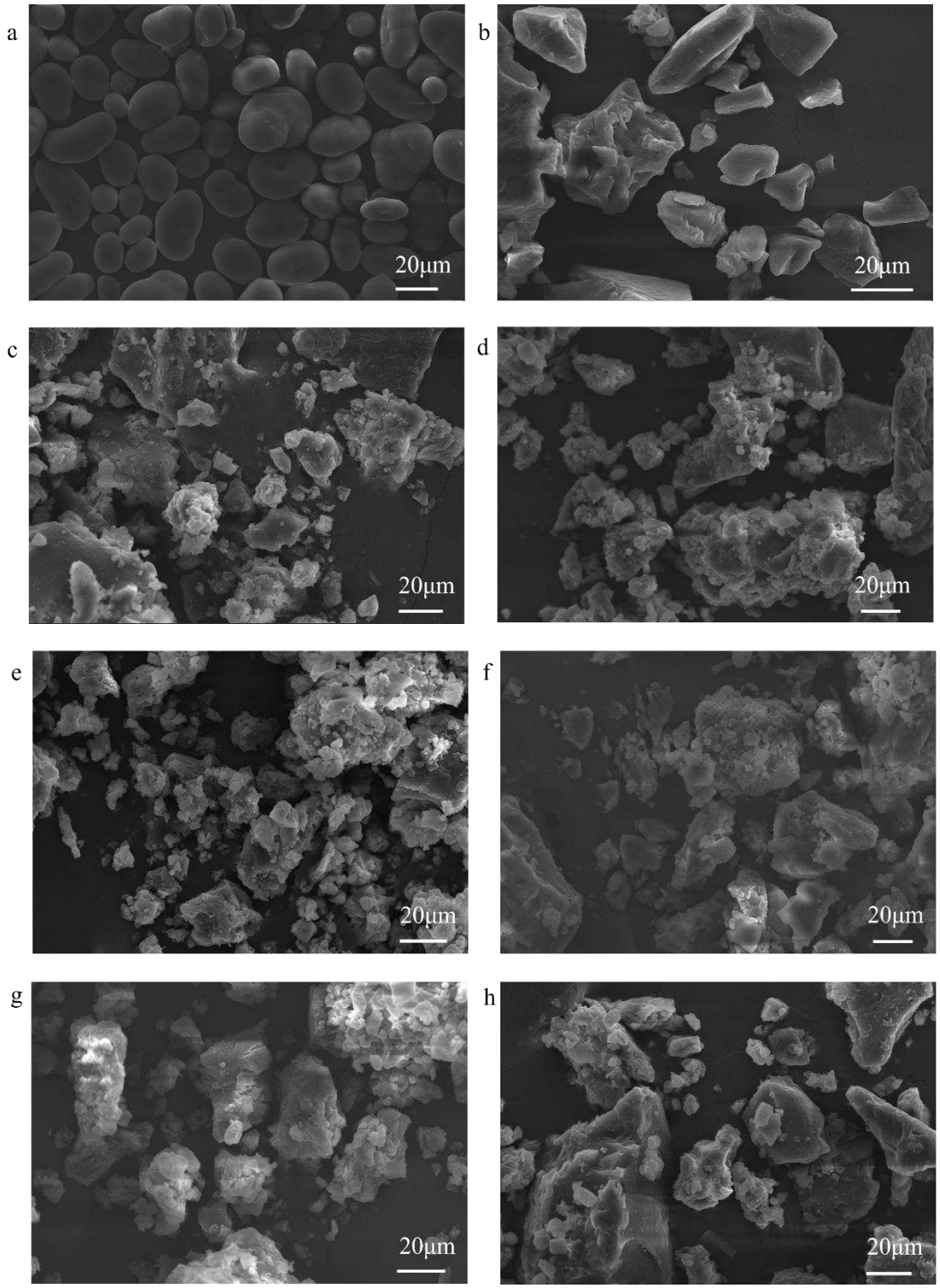


Fig. 3 Scanning electron micrographs (SEM) of PS, DPS, and DPS-OA complexes. (a) PS; (b) DPS; (c) DPS-1.5%OA; (d) DPS-3%OA; (e) DPS-6% OA; (f) DPS-9% OA; (g) DPS-12%OA; (h) DPS-15%OA.

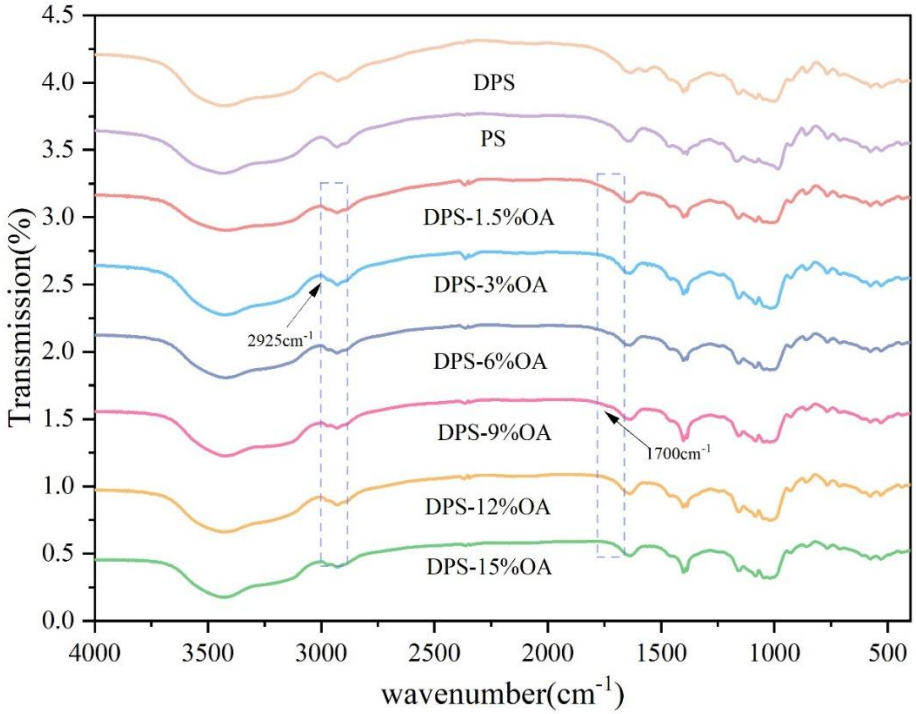
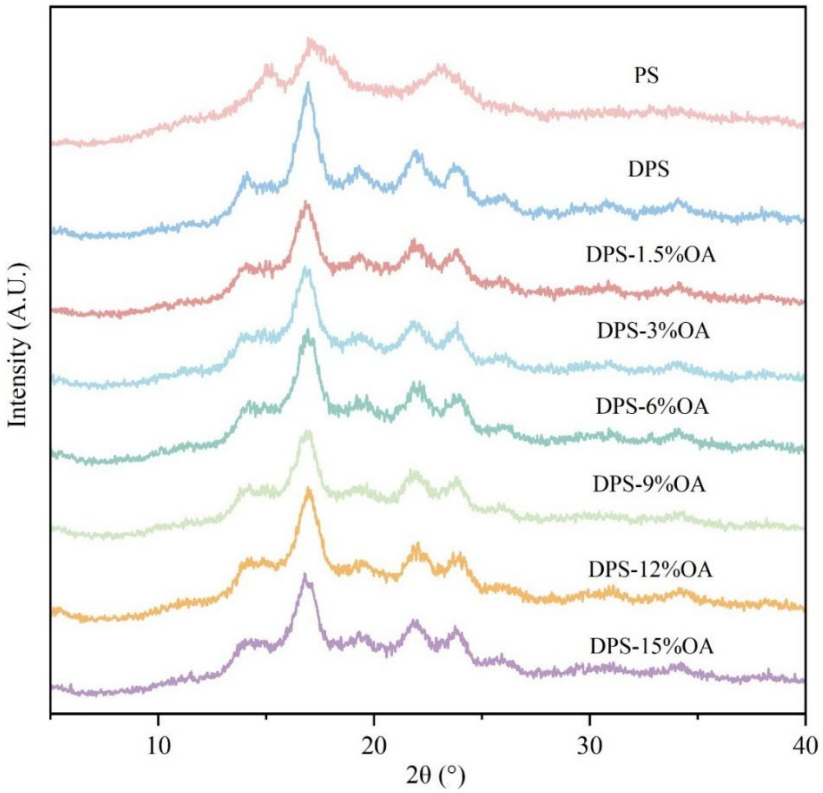


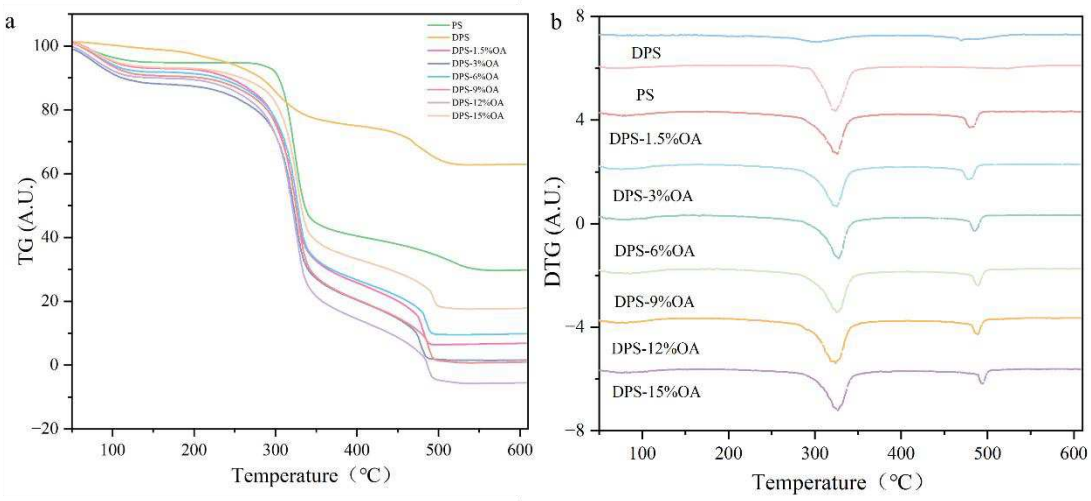
Fig. 4. FTIR spectra of PS, DPS, and DPS-OA complexes.



809

810 Fig. 5. XRD patterns of PS, DPS, and DPS-OA complexes.

811

812 

813 Fig. 6. TG curves (a) and DTG curves (b) curves of PS, DPS, and DPS-OA complexes.

814

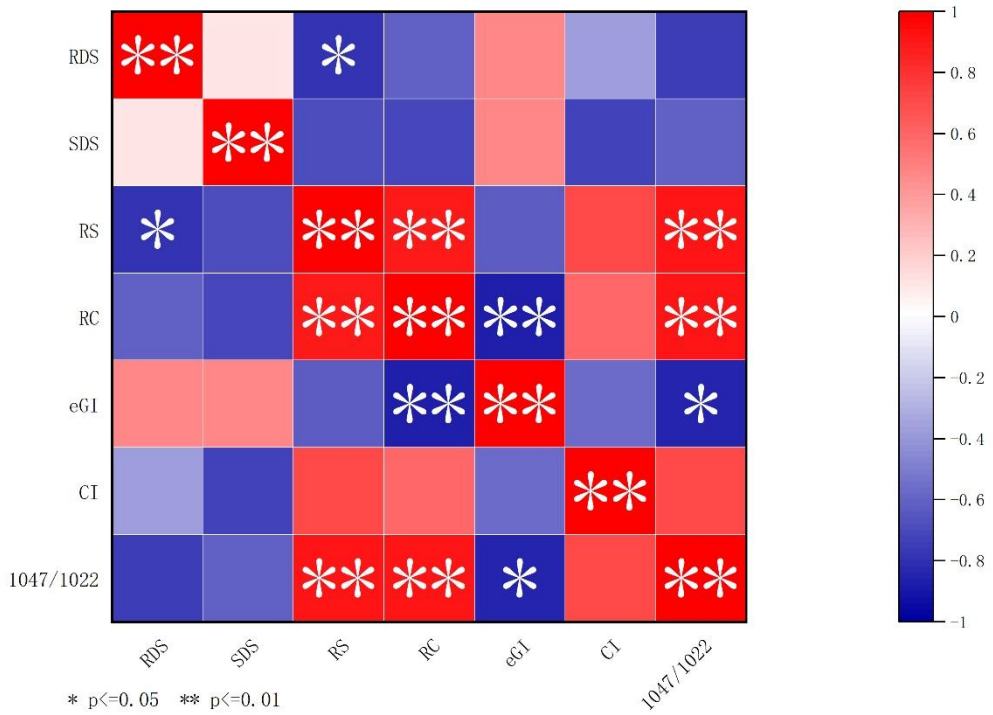


Fig. 7. Correlation analysis of the CI, multi-scale structure, and in-vitro digestibility of DPS-OA complexes with different OA concentrations. RDS: rapidly digestible starch; SDS: slowly digestible starch; RS: resistant starch; eGI: estimated glycemic index; RC: relative crystallinity.

822 Table 1. In vitro digestion properties of PS, DPS, and DPS-OA complexes.

Samples	RDS（%）	SDS（%）	RS（%）
PS	60.31±0.67^{a}	25.09±0.48^{ab}	14.60±0.19^{f}
DPS	31.75±1.84^{b}	26.65±0.65^{ab}	41.60±1.20^{e}
DPS-1.5%OA	23.35±1.39^{cd}	29.35±3.60^{a}	47.29±4.92^{cd}
DPS-3%OA	26.85±0.80^{c}	22.86±2.36^{b}	50.29±3.05^{bc}
DPS-6%OA	20.92±1.95^{d}	23.79±0.75^{b}	55.29±1.67^{a}
DPS-9%OA	24.00±1.43^{b}	23.96±0.97^{b}	52.05±1.17^{ab}
DPS-12%OA	26.49±3.25^{c}	29.16±3.75^{a}	44.34±1.62^{de}
DPS-15%OA	30.38±2.81^{cd}	26.03±2.54^{ab}	43.59±0.28^{de}

823 Note: Means ± standard deviations of triplicate analyses are given. The letters (a-f)
824 manifest significant ($p < 0.05$) difference among the same column.
825

826 Table 2.RC, short-range molecular order, and eGI of PS, DPS, and DPS-OA

827 complexes.

Samples	RC(%)	1047/1022	eGI
PS	12.37 ± 0.34^{f}	1.001 ± 0.001^{f}	57.60 ± 0.25^{a}
DPS	18.94 ± 0.18^{a}	1.008 ± 0.003^{e}	39.19 ± 0.55^{b}
DPS-1.5%OA	14.51 ± 0.40^{e}	1.007 ± 0.006^{e}	34.45 ± 0.33^{c}
DPS-3%OA	16.16 ± 0.63^{cd}	1.015 ± 0.002^{c}	33.56 ± 0.27^{d}
DPS-6%OA	17.65 ± 0.28^{b}	1.040 ± 0.001^{a}	30.91 ± 0.98^{f}
DPS-9%OA	16.57 ± 0.06^{c}	1.038 ± 0.003^{b}	31.64 ± 0.30^{f}
DPS-12%OA	15.51 ± 0.22^{d}	1.010 ± 0.002^{d}	32.50 ± 0.37^{e}
DPS-15%OA	14.65 ± 0.84^{e}	1.001 ± 0.004^{f}	33.37 ± 0.17^{d}

828 Note: Means ± standard deviations of triplicate analyses are given. The letters (a-f)

829 manifest significant ($p < 0.05$) difference among the same column.

Supplementary Files

This is a list of supplementary files associated with this preprint. Click to download.

- highlights.docx
- Graphicalabstract.docx